Solid State ^{15}N NMR and Theoretical Studies of Primary and Secondary Geometric H/D Isotope Effects on Low-Barrier NHN−Hydrogen Bonds

Hans Benedict,[†] Hans-Heinrich Limbach,*[,†] Martin Wehlan,[‡] Wolf-Peter Fehlhammer,[‡] Nicolai S. Golubev,[§] and Rudolf Janoschek*[,⊥]

Contribution from the Institut für Organische Chemie, Takustrasse 3, and Institut für Anorganische Chemie der Freien Universität Berlin, Fabeckstrasse 34/36, D-14195 Berlin, Germany, Institute of Physics, St. Petersburg State University, 198904 St. Petersburg, Russian Federation, and Institut für Theoretische Chemie der Karl-Franzens Universität Graz, Strassoldogasse 10, A-8010 Graz, Austria

Received June 16, 1997. Revised Manuscript Received December 15, 1997

Abstract: Using a combination of high resolution and dipolar solid state ^{15}N NMR we have determined H/D isotope effects on the nitrogen-hydron (L = H, D) distances and ^{15}N chemical shielding tensors of strongly hydrogen bonded bisisocyanide salts of the type $[(CO)_5Cr-C{\equiv}N\cdots L\cdots N{\equiv}C-Cr(CO)_5]^-\ X^+$, where $X^+ = AsPh_4^+$ (**2**) and $X^+ = NPr_4^+$ (**3**). These compounds have been modeled theoretically by the linear system $[C{\equiv}N\cdots L\cdots N{\equiv}C]^-Li^+$ (**1**). The crystal field acting on the anion was generated by a variety of fixed C···Li distances. For the calculation of dynamical corrections of geometries and NMR chemical shifts, an iterative procedure based on the crude adiabatic approximation was employed, consisting of (i) ab initio calculation of the energy hypersurface at the MP2/6-31+G(d,p) level, (ii) solution of the Schrödinger equation for the anharmonic collinear hydron motion, and (iii) NMR chemical shift calculations using the IGLO-method. The two hydrogen bond distances $r_1 \equiv N\cdots L$ and $r_2 \equiv L\cdots N$ are found to change in a correlated way when H is replaced by D, as a function of X^+, i.e., of the electric field at the hydrogen bond site. The correlation $r_1 = f(r_2)$ established here experimentally and theoretically for very strong NHN-hydrogen bonds shows a good agreement with a correlation established previously (Steiner, Th. *J. Chem. Soc., Chem. Commun.* ***1995,*** 1331) based on the neutron diffraction structures of a number of weakly hydrogen bonded solids. A plot of the sum $q_2 = r_1 + r_2$—corresponding in a linear hydrogen bond to the heavy atom separation—as a function of the proton dislocation from the hydrogen bond center $q_1 = {}^1/_2(r_1-r_2)$ exhibits a minimum value at about 2.54 Å for the symmetric low-barrier hydrogen bond at $q_1 = 0$. This situation is realized experimentally for **2**. When $q_1 \neq 0$ anharmonic single well hydrogen bonds are obtained, typical for **3**. The geometric H/D isotope effects can be split into a *primary* effect referring to the hydron position $q_1 = {}^1/_2(r_1-r_2)$ and a *secondary* effect referring to the heavy atom position q_2. Secondary effects have been reported previously by Ubbelohde. Both isotope effects are shown to be related in a simple empirical way to the hydrogen bond geometries and to the isotopic fractionation factors. Finally, it is shown that the chemical shielding of the nuclei in the hydrogen bridge is a qualitative probe for the *primary* and *secondary* geometric isotope effects.

Introduction

Proton transfer in hydrogen bonded systems is an important phenomenon in chemistry and biology of acids and bases.[1−6] Generally, it is regarded as a rate process involving a barrier for the proton motion, leading to kinetic H/D isotope effects.[2] However, a number of hydrogen bonded systems are now known where the proton motion experiences only a very low barrier, leading to a proton delocalization in the hydrogen bond which strongly depends on the environment.[5q,6] Such low-barrier hydrogen bonds have been discussed as intermediates or transition states of enzymic catalysis;[5] in this case kinetic isotope effects will be smaller as compared to the high-barrier case. However, other isotopic techniques can be used to study low-barrier hydrogen bonds. For example, Kreevoy and Liang have studied H/D-fractionation factors in various hydrogen bonded acid−base complexes dissolved in organic liquids as a function of the acidity of the proton donor;[7a] these factors reflect changes of proton zero-point energy, i.e., of its bonding characteristics.[7b,c] Recently, this phenomenon has been described theoretically by

[†] Institut für Organische Chemie der Freien Universität Berlin.
[‡] Institut für Anorganische Chemie der Freien Universität Berlin.
[§] St. Petersburg State University.
[⊥] Institut für Theoretische Chemie der Karl-Franzens Universität Graz.

(1) (a) *The Hydrogen Bond;* Schuster, P.; Zundel, G.; Sandorfy, C., Eds.; North-Holland Publ. Co.: Amsterdam, 1976. (b) Jeffrey, G. A.; Saenger, W. *Hydrogen Bonding in Biological Structures*, Springer-Verlag: Berlin, 1991. (c) Bell, R. P. *The Proton in Chemistry*, 2nd ed.; Chapman and Hall: London, 1973.

(2) (a) Limbach, H. H. Dynamic NMR Spectroscopy in the Presence of Kinetic Isotope Effects. Chapter 2 In *NMR Basic Principles and Progress*; Springer, Berlin, 1991; Vol. 26; pp 63−164. (b) Smith, J. A. S.; Wehrle, B.; Aguilar-Parrilla, F.; Limbach, H. H.; Foces-Foces, M. C.; Cano, F. H.; Elguero, J.; Baldy, A.; Pierrot, M.; Khurshid, M. M. T.; Larcombe-McDuall, J. B. *J. Am. Chem. Soc.* **1989**, *111*, 7304. (c) Schlabach, M.; Wehrle, B.; Braun, J.; Scherer, G.; Limbach, H. H. *Ber. Bunsen-Ges. Phys. Chem.* **1992**, *96*, 821. (d) Braun, J.; Schlabach, M.; Wehrle, B.; Köcher, M.; Vogel, E.; Limbach, H. H.; *J. Am. Chem. Soc.* **1994**, *116*, 6593. (e) Aguilar-Parilla, F.; Scherer, G.; Limbach, H. H.; Foces-Foces, M. C.; Cano, F. H.; Smith, S. A. S.; Toiron, C.; Elguero, J. *J. Am. Chem. Soc.* **1992**, *114*, 9657. (f) Hoelger, Ch.; Wehrle, B.; Benedict, H.; Limbach, H. H. *J. Phys. Chem.* **1994**, *98*, 843. (g) J. Braun, R. Schwesinger, P. G.; Williams, H. Morimoto, D. E.; Wemmer, H. H.; Limbach, *J. Am. Chem. Soc.*, in press.

S0002-7863(97)01979-3 CCC: $15.00
Published on Web 03/17/1998

Scheme 1

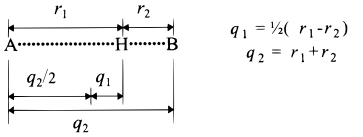

Huskey.[7d] On the other hand, the hydrogen bond geometries depend not only on the chemical and the crystal structure[8] but also on the replacement of the hydrogen bond proton by a deuteron. Such geometric isotope effects of low-barrier hydrogen bonds are not yet well understood and constitute the topic of this paper.

As indicated in Scheme 1, the two bonds of a hydrogen bonded system can be characterized by the two distances r_1 and r_2 or alternatively by the coordinates $q_1 = {}^1/_2(r_1-r_2)$ and $q_2 = r_1 + r_2$. In the case of a linear hydrogen bond q_1 represents the deviation of the proton from the hydrogen bond center and q_2 the heavy atom distance A···B. One can then define a *primary* geometric H/D isotope effect referring to the different position of the proton and the deuteron, i.e., the different values of q_1 for both particles, and a *secondary* geometric H/D isotope effect referring to the change of q_2, i.e., of the heavy atom locations by deuteration. Secondary effects were reported by Ubbelohde[9] for a number of solids, exhibiting however a large number of strongly coupled hydrogen bonds. Because of the problems of X-ray diffraction to localize protons and of the special requirements of neutron diffraction, the evaluation of primary geometric H/D isotope effects by these methods is difficult.[3] In principle, isolated hydrogen bonds could be studied by placing the systems in a solid or liquid matrix, but then the determination of geometric H/D isotope effects is even more difficult. For the liquid state, the evaluation of isotope effects on NMR chemical shifts has been established as a tool in order to obtain qualitative information about intramolecular geometries,[12] and this method has, therefore, also been applied to characterize intramolecular hydrogen bonds.[13] With the exception of the very stable FHF^-/FDF^- anions[13a] the NMR method has only been applied very recently to evaluate geometric isotope effects of intermolecular hydrogen bonded acid−base complexes,[13b] because the slow hydrogen bond exchange region can only be reached at low temperatures using special solvents.[5o,p,13c,d] On the other hand, liquid state NMR still refers to hydrogen bonded systems experiencing an averaged solvent shell, a problem which does not arise when studying crystalline solids using advanced NMR methods. E.g., in the past years especially dynamic high-resolution solid state ^{15}N NMR spectroscopy under the conditions of cross-polarization (CP) and magic angle spinning (MAS) has been shown to be a convenient tool for the study of the kinetics of proton and deuteron transfer from and to nitrogen.[2]

Scheme 2

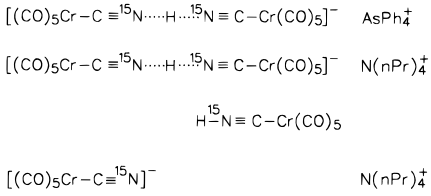

Using this method, we have recently[14] observed for the first time H/D isotope effects on the solid state ^{15}N NMR chemical shifts of a series of homoconjugate model complexes **2** and **3** depicted in Scheme 2 whose syntheses and structures were described previously.[15] It is noteworthy that the distance N···N in **2** was found by X-ray analysis to be only 2.57 Å which is very short for intermolecular N···H···N hydrogen bonds.[1,3] By ^{15}N CPMAS NMR investigation of the ^{15}N labeled materials it was found that the symmetry of the low barrier N···H···N^- hydrogen bond is perturbed when the countercation X^+ is varied. Thus, in the case of **2** the hydrogen bonded system was found

(3) (a) Novak, A. *Struct. Bonding (Berlin)* **1974**, *18*, 177. (b) Olovsson, I.; Jönsson, P. G. ref 1a, Chapter 8, pp 393−456. (c) Trueblood, K. N. In *Accurate Molecular Structures, Their Determination and Importance*; Domenicano, A., Hargittai, I., Eds.; Oxford Univ. Press: 1992; Chapter 8, p 200. (d) Jones, D. J.; Brach, I.; Roziere, J. *J. Chem. Soc., Dalton Trans.* **1984**, 1795. (e) Boenigk, D.; Mootz, D. *J. Am. Chem. Soc.* **1988**, *110*, 2135. (f) Emsley, J.; Jones, D. J.; Lucas, J. *Rev. Inorg. Chem.* **1981**, *3*, 105. (g) Ault, B. S. *Acc. Chem. Res.* **1982**, *15*, 103. (h) Mootz, D.; Bartmann, K. *Angew. Chem.* **1988**, *100*, 424; *Angew. Chem., Int. Ed. Engl.* **1988**, *27*, 391. (i) Berthold, H. J.; Preibsch, E.; Vonholdt, E. *Angew. Chem.* **1988**, *100*, 1581; *Angew. Chem., Int. Ed. Engl.* **1988**, *27*, 1527. (j) Hibbert, F.; Emsley, J. *Adv. Phys. Org. Chem.* **1990**, *26*, 255.

(4) (a) Samorjai, R. L.; Hornig, D. F. *J. Chem. Phys.* **1962**, *36*, 1980. (b) Janoschek, R.; Weidemann, E. G.; Pfeiffer, H.; Zundel, G. *J. Am. Chem. Soc.* **1972**, *94*, 2387.

(5) (a) Swain, C. G.; Kuhn, D. A.; Schowen, R. L. *J. Am. Chem. Soc.* **1965,** *87*, 1553. (b) Eliason, R.; Kreevoy, M. M. *J. Am. Chem. Soc.* **1978**, *100*, 7037. (c) Hadzi, D. Proton Transfers in Biological Mechanisms. *J. Mol. Struct.* **1988**, *177*, 1. (d) Cleland, W. W.; Kreevoy, M. M. *Science* **1994**, *264*, 1887. (e) Cleland, W. W.; Kreevoy, M. M. *Science* **1995**, *269*, 104. (f) Perrin, C. L. *Science* **1994**, *266*, 1665. (g) Blow, D. M.; Birktoft, J. J.; Hartley, B. S. *Nature* **1969**, *221*, 337. (h) Blow, D. M.; Steitz, T. A. *Annu. Rev. Biochem.* **1970**, *39*, 63. (i) Schowen, R. L. In *Mechanistic Principles of Enzyme Activity*; Liebman, J. F., Greenberg, A., Eds.; 1988; VCH Publishers: New York, p 119. (j) Schowen, K. B.; Schowen, R. L. *Methods Enzymol.* **1982**, *87*, 551. (k) Venkatasubban, K. S.; Schowen, R. L. *CRC Crit. Rev. Biochem.* **1984**, *17*, 1. (l) Cook, P. F. *Enzyme Mechanisms from Isotope Effects*; CRC Press: New York, 1992; (m) Frey, P. A.; Whitt, S. A.; Tobin, J. B. *Science* **1994**, *264*, 1927. (n) Frey, P. A. *Science* **1995**, *265*, 104. (o) Denisov, G. S.; Golubev, N. S.; Gindin, V. A.; Limbach, H. H.; Ligay, S. S.; Smirnov, S. N. *J. Mol. Struct.* **1994**, *322*, 83. (p) Golubev, N. S.; Gindin, V. A.; Ligay, S. S.; Smirnov, S. N. *Biochemistry (Moscow)* **1994**, *59*, 447. (q) Warshel, A; Papazyan, A.; Kollman, P. A. *Science* **1995**, *269*, 102. (r) Shan, S.; Loh, S.; Herschlag, D. *Science* **1996**, *272*, 97.

(6) Scheiner, S.; Kar, T. *J. Am. Chem. Soc.* **1995**, *117*, 6970.

(7) (a) Kreevoy, M. M.; Liang, T. M. *J. Am. Chem. Soc.* **1980,** *102*, 361. (b) Bigeleisen, J.; Wolfsberg, M. *Adv. Chem. Phys.* **1958**, *1*, 15. (c) More O'Ferrall, R. A. *Substrate Isotope Effects*, in *Proton-Transfer Reactions*; Caldin, E. F., Gold, V., Eds.; Chapman and Hall: London, 1975; Chapter 8, pp 201−262. (d) Huskey, P. W. *J. Am. Chem. Soc.* **1996**, *118*, 1663.

(8) (a) Steiner, Th.; Saenger, W. *Acta Crystallogr.* **1994**, *B50*, 348. (b) Steiner, Th. *J. Chem. Soc., Chem. Commun.* **1995**, 1331. (c) Gilli, P.; Bertolasi, V.; Ferretti, V.; Gilli, G. *J. Am. Chem. Soc.* **1994**, *116*, 909.

(9) Ubbelohde, A. R.; Gallagher, K. G. *Acta Crystallogr.* **1955**, *8*, 71.

(10) (a) Legon, A. C.; Millen, D. J. *Chem. Phys. Lett.* **1988,** *147*, 484. (b) Sokolov, N. D., Savel'ev, V. A. *Chem. Phys.* **1977,** *22*, 383. (c) Sokolov, N. D.; Savel'ev, V. A. *Chem. Phys.* **1994,** *181*, 305. (d) Almlöf, J. *Chem. Phys. Lett.* **1972**, *17*, 49.

(11) Hansen, P. E. Isotope Effects in Nuclear Shielding. *Prog. NMR Spectrosc.* **1988**, *20*, 207.

(12) (a) Altman, L. J.; Laungani, D.; Gunnarson, G.; Wennerström, H.; Egan, W.; Forsén, S. *J. Am. Chem. Soc.* **1978,** *100*, 8264. (b) Hansen, P. E. *J. Mol. Struct.* **1994**, *321*, 79. (c) Hansen, P. E.; Lycka, A. *Acta Chem. Scand.* **1989**, *43*, 222. (d) Hansen, P. E.; Kawecki, R.; Krowczynski, A.; Kozerski, L. *Acta Chem. Scand.* **1990**, *44*, 826. (e) Munch, M.; Hansen, A. E.; Hansen, P. E.; Bouman, T. D. *Acta Chem. Scand.* **1992**, *46*, 1065. (f) Hansen, P. E.; Christoffersen, M.; Bolvig, S. *Magn. Reson. Chem.* **1993**, *31*, 893.

(13) (a) Fujiwara, F. Y.; Martin, J. S. *J. Am. Chem. Soc.* **1974**, *96*, 7625. (b) Smirnov, S. N.; Golubev, N. S.; Denisov, G. S.; Benedict, H.; Schah-Mohammedi, P.; Limbach, H.-H. *J. Am. Chem. Soc.* **1996**, *118*, 4094. (c) Golubev, N. S.; Smirnov, S. N.; Gindin, V. A.; Denisov, G. S.; Benedict, H.; Limbach, H.-H. *J. Am. Chem. Soc.* **1994**, *116*, 12055. (d) Golubev, N. S.; Denisov, G. S.; Smirnov, S. N.; Shchepkin, D. N.; Limbach, H. H. *Z. Phys. Chem.* **1996**, *196*, 73.

(14) Benedict, H.; Hoelger, C.; Aguilar-Parrilla, F.; Fehlhammer, W. P.; Wehlan, M.; Janoschek, R.; Limbach, H.-H. *J. Mol. Struct.* **1996**, *378*, 11.

(15) Bär, E.; Fuchs, J.; Kolrep, T.; Rieger, D.; Aguilar-Parrilla, F.; Limbach, H. H.; Fehlhammer, W. P. *Angew. Chem.* **1991**, *103*, 88; *Angew. Chem., Int. Ed. Engl.* **1991**, *30*, 80.

to be symmetric, whereas in the case of **3** it was asymmetric. The H/D isotope effects on the ^{15}N chemical shifts were small in the symmetric and large in the asymmetric case. These effects were studied theoretically by means of ab initio calculations of the simpler complex **1**. However, a quantitative comparison of theoretical and experimental geometric H/D isotope effects was still lacking. This problem could now be solved in two different ways. First, some of us have shown recently[17] that dipolar solid state ^{15}N NMR can be used in order to obtain both *primary* and *secondary* H/D isotope effects on the geometries of hydrogen bonds from and to nitrogen. In previous studies dipolar interactions have been exploited in order to measure separately ^{15}N−H distances[18] and one ^{15}N−D distance[19] but no H/D isotope effects on nitrogen-hydron distances. The determination of such effects requires a high precision which is not easily obtained. By a special stratagem we succeeded here nevertheless to measure such effects in the case of the low-barrier hydrogen bond of polycrystalline **2** and **3**. It will be shown that these systems represent a missing link in a correlation of covalent and hydrogen bond length in NHN-hydrogen bonded systems found by Steiner;[8b] moreover, this correlation is now reproduced theoretically. On the other hand, we have extended the preliminary computational results concerning the influence of the hydrogen bond geometric isotope effects on calculated NMR chemical shifts of **1**.[14]

This paper is organized as follows. In a short theoretical section we describe the way how to obtain hydrogen bond distances by dipolar NMR as well as the theoretical procedure to model compound **1**. Then, the results of the NMR experiments and the theoretical calculations will be presented and discussed.

Methods

Experimental. ^{15}N labeled **2-*h*** and **3-*h*** were synthesized from KC^{15}N as described previously.[15] Deuteration of the hydrogen bridge, leading to **2-*d*** and **3-*d*,** was performed by repeated dissolving **2-*h*** and **3-*h***, respectively, in methanol-*d* and evaporating the solvent. To prevent reprotonation, the samples were transferred into MAS rotors and sealed under nitrogen gas.

All ^{15}N CP NMR measurements were performed at 9.12 MHz (2.1 T cryomagnet) using a Bruker CXP 100 spectrometer equipped with a Doty 7 mm standard CPMAS probe. A standard CP pulse sequence was used. The 90° pulse width was 4.5 μs, the contact pulse width was between 2 and 8 ms, and the recycle time was 3 s. All spectra are referenced to external solid $^{15}NH_4Cl$ (95%). Some of the spectra were performed at low temperatures (160−170 K), but no spectral changes could be observed.

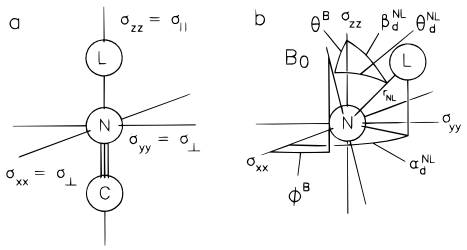

Figure 1. (a) Orientation of the CSA tensor relative to the molecular coordinate system in the model compounds **1-*h***, **1-*d***, and **4**. (b) Orientation of the N−L bond vector and the magnetic field B_0 in the principal axis system of the tensor for the chemical shift anisotropy (CSA).

Determination of N···H/N···D Distances by Dipolar ^{15}N Solid-State NMR. The NMR theory of dipolar heteronuclear coupling[21] between nuclei N≡^{15}N and L = H, D has been reviewed recently.[17] Therefore, only some definitions needed in the context of this work will be shortly reviewed here.

The absorption frequency ν^N of a ^{15}N nucleus embedded in a given crystallite can be described by

$$\nu^N = \nu^N_{ZEE} + \nu^N_{CSA} + \sum_L m_L \nu^{NL}_d \quad (1)$$

Here, ν^N_{ZEE} represents the ^{15}N Zeeman frequency, ν^N_{CSA} the chemical shift anisotropy (CSA), ν^{NL}_d the dipolar coupling frequency between ^{15}N and the light isotopes (hydrons) L = H, D, and m_L the magnetic quantum number of the dipolar coupled hydrons L. The Zeeman frequency depends on the gyromagnetic ratio γ^N and the strength of the applied external magnetic field B_0, i.e.

$$\nu^N_{ZEE} = \frac{\gamma^N B_0}{2\pi} \quad (2)$$

The CSA contribution can be described in terms of the principle components of a tensor σ illustrated in Figure 1a, i.e.

$$\nu^N_{CSA} = \nu^N_{ZEE}(\sigma_{XX}\cos^2\phi^B \sin^2\theta^B + \sigma_{YY}\sin^2\phi^B \sin^2\theta^B + \sigma_{ZZ}\cos^2\theta^B) \quad (3)$$

Here, ϕ^B and θ^B are the Euler angles describing the orientation of the external magnetic field B_0 relative to the principal axis system of the σ tensor of ^{15}N, as depicted in Figure 1b. The value of the isotropic chemical shift σ_{iso} that is obtained when the anisotropy is eliminated by molecular motion in liquids or by fast rotation of a macroscopic powder sample about an axis that has the "magic angle" of 54.7° to the external magnetic field (magic angle spinning = MAS) is given by

$$\sigma_{iso} = (\sigma_{XX} + \sigma_{YY} + \sigma_{ZZ})/3 \quad (4)$$

As the σ tensor is a molecular property, the orientation of the principal axis system of the tensor is fixed relative to the

(16) Frisch, M. J.; Trucks, G. W.; Schlegel, H. B.; Gill, P. M. W.; Johnson, B. G.; Robb, M. A.; Cheeseman, J. R.; Keith, T.; Petersson, G. A.; Montgomery, J. A.; Raghavachari, K.; Al-Laham, M. A.; Zakrzewski, V. G.; Ortiz, J. V.; Foresman, J. B.; Cioslowski, J.; Stefanov, B. B.; Nanayakkara, A.; Challacombe, M.; Peng, C. Y.; Ayala, P. Y.; Chen, W.; Wong, M. W.; Andres, J. L.; Replogle, E. S.; Gomperts, R.; Martin, R. L.; Fox, D. J.; Binkley, J. S.; Defrees, D. J.; Baker, J.; Stewart, J. P.; Head-Gordon, M.; Gonzalez, C.; Pople, J. A. Gaussian-92; Gaussian, Inc.: Pittsburgh, PA, 1992.

(17) (a) Hoelger, C. G.; Limbach, H. H. *J. Phys. Chem.* **1994**, *98*, 11803. (b) Hoelger, C. G.; Limbach, H. H.; Aguilar-Parrilla, F.; Elguéro, J.; Weintraub, O.; Vega, S. *J. Magn. Reson.* **1996**, *A120*, 46.

(18) (a) Stoll, M. E.; Vega, A. J.; Vaughan, R. W. *J. Chem. Phys.* **1976**, *65*, 4093. (b) Roberts, J. E.; Harbison, G. S.; Munowitz, M. G.; Herzfeld, J.; Griffin, R. G. *J. Am. Chem. Soc.* **1987**, *109*, 4163. (c) Tekely, P.; Montigny, F.; Canet, F.; Delpuech, J. J. *Chem. Phys. Lett.* **1990**, *175*, 401. (d) Munowitz, M. G.; Griffin, R. G. *J. Chem. Phys.* **1982**, *76*, 2848. (e) Munowitz, M. G.; Aue, W. P.; Griffin, R. G. *J. Chem. Phys.* **1982**, *77*, 1686.

(19) Hiyama, Y.; Niu, C. H.; Silverton, J. V.; Bavoso, A.; Torchia, D. A. *J. Am. Chem. Soc.* **1988**, *110*, 2378.

(20) Kutzelnigg, W.; Fleischer, U.; Schindler, M. The IGLO Method: Ab initio Calculation and Interpretation of NMR Chemical Shifts and Magnetic Susceptibilities. Chapter 3 In *NMR Basic Principles and Progress*; Springer: Berlin, 1991; Vol. 23, pp 165−262.

(21) (a) Mehring, M. High-Resolution NMR in Solids. In *NMR BasicPrinciples and Progress*, 2nd ed.; Springer: Berlin−Heidelberg−New York, 1978; Vol. 11. (b) Sethi, N. K.; Aldermann, D. W.; Grant, D. M. *Mol. Phys.* **1990**, *71*, 217. (c) Zilm, K. W.; Grant, D. M. *J. Am. Chem. Soc.* **1981**, *103*, 2913.

molecular frame. In case of axially symmetric molecular segments such as RN···H···NR$^-$ found in compounds **1**−**3** the σ tensors of the nuclei in this segments are axially symmetric as well. Thus, the component of the CSA tensor parallel to the molecular symmetry axis is given by $\sigma_{ZZ} = \sigma_{\parallel}$ and the perpendicular components by $\sigma_{XX} = \sigma_{YY} = \sigma_{\perp}$ as shown in Figure 1a. The dipolar frequency is given by

$$\nu_d^{NL} = D^{NL}(1-3\cos^2\theta_d^{NL}), \quad D^{NL} = \frac{\gamma^N\gamma^L h\mu_0}{16\pi^3 r_c^3(NL)} \quad (5)$$

D^{NL} is the dipolar coupling constant, γ^N and γ^L are the gyromagnetic ratios of the two nuclei, h Planck's constant, μ_0 the magnetic permeability. $r_c(NL)$ represents the mean cubic internuclear distance N···L given by

$$r_c(NL) = \langle\Psi|\hat{r}^{-3}(NL)|\Psi\rangle^{-1/3} \quad (6)$$

where Ψ represents the spatial nuclear wave function and $\hat{r}^{-3}(NL)$ the reciprocal cubic distance operator. If $r_c(NL)$ is expressed in Å it follows that

$$D^{NH} = 12158 r_c^{-3}(NH)[Hz] \quad \text{and}$$
$$D^{ND} = 1868 r_c^{-3}(ND)[Hz] \quad (7)$$

In eq 5, θ_d^{NL} is the angle between the magnetic field and the vector NL as depicted in Figure 1b. As can be inferred from Figure 1b, this angle can more conveniently be described by the Euler angles in the coordinate system of the CSA tensor—ϕ^B and θ^B for the magnetic field and α_d^{NL} and β_d^{NL} for the vector NL, respectively. It can be shown that

$$\cos\theta_d^{NL} = \sin\beta_d^{NL}\sin\theta^B\cos(\phi^B - \alpha_d^{NL}) + \cos\beta_d^{NL}\cos\theta^B \quad (8)$$

The ^{15}N NMR spectrum of a polycrystalline powder is obtained from eqs 1−8 by calculating ν^N for all possible orientations by variation of ϕ^B and θ^B using increments of 1−2°. For statistical reasons the signal intensity has to be weighted by a factor of $\sin\theta^B$.

Experimentally, only relative chemical shifts $\delta = \sigma_{ref} - \sigma$, which are measured with respect to some standard, can be obtained. For the determination of the ^{15}N···D distances first the elements of the ^{15}N CSA tensor are determined by simulating the experimental solid state ^{15}N NMR spectrum of the protonated system, i.e., L = H, under proton decoupling. The values obtained are then used for a first simulation of the proton decoupled ^{15}N NMR spectrum of the species deuterated in the hydrogen bond, by adapting the remaining parameters α_d^{ND}, β_d^{ND}, and D^{ND}. Finally, a fine-tuning of all parameters is performed revealing major H/D isotope effects on the elements of the ^{15}N CSA tensor. The determination of the ^{15}N···H distances is more difficult, as ^{1}H homodecoupling has to be applied introducing a scaling factor of the dipolar ^{15}N−H coupling which has to be determined in a separate experiment.[18] Here, we could obtain the distances N···H by extrapolation from the observed strong dependence of the N···D distances on the isotropic chemical shifts.

Quantum Mechanical Calculations. As polycrystalline **2** and **3** are too large for a full ab initio treatment, all calculations were done on the simplified linear system [C1≡N1···L···N2≡C2]$^-$ Li$^+$ **1-*h*, 1-*d*** (see Scheme 2). The influence of the electric field of different counterions X$^+$ on the anion was modeled by a variety of fixed distances C2···Li.

In principle, a rigorous theoretical treatment of the anharmonic molecular motion is required for estimating dynamical corrections and isotope effects. For H-bonded systems the anharmonic investigation of the collinear motion of the hydron demands the least effort.[1,4] Moreover, as the model compound **1** constitutes only an approximation for **2** and **3** anyway, we restrict our calculations of dynamical corrections for the interatomic distances to $r_1 \equiv$ N1···L and $r_2 \equiv$ L···N2 or to the coordinates q_1 and q_2 as defined in Scheme 1, using the crude adiabatic approximation. This approximation is justified because of the slow N1−N2 motion (≈275 cm^{-1}, calculated) compared with the collinear proton motion (≈1329 cm^{-1}, calculated) in the anion of **1-*h***, at a distance C2···Li → ∞. The application of this approximation consisted in an iterative procedure for the calculation of the dynamically corrected interatomic distances as is described as follows.[14] (i) The potential energy function $V(q_1)$ for the collinear hydron motion is calculated pointwise at fixed optimized heavy atom positions. These calculations were performed at the MP2/6-31+G(d,p) level using the GAUSSIAN 92 program package.[16] (ii) The one-dimensional Schrödinger equation for the anharmonic collinear hydron motion is solved separately for L = H and D using known methods.[4a,b] For simplicity the masses of the heavy atoms are set to infinity. The expectation value $\langle\Psi_0|q_1|\Psi_0\rangle$, where $\Psi_0(q_1)$ represents the anharmonic vibrational ground-state wave function of the hydron, is used for calculating the distance $r_1 \equiv$ N1···L. (iii) The heavy atom coordinates are reoptimized keeping the distance C2···Li and the dynamically corrected N1···L distance constant. This procedure is repeated until self-consistency is achieved; a convergence criterion of 10^{-3} Å was used. In this way the dynamically corrected vibrational wave functions of the proton and the deuteron and the corresponding energies were obtained. Using this information the zero-point energy differences ΔZPE between the protonated and the deuterated hydrogen bond (neglecting bending contributions) and the mean linear and cubic average distances N1···L and N2···L were calculated for the vibrational ground state, for comparison with the experimental values (see eq 6).

The calculation of the elements of NMR shielding tensors and the resulting isotropic chemical shifts was performed by the IGLO (Individual Gauge for Localized Orbitals) method employing the basis set II.[20] Absolute shielding values $\sigma(q_1)$ were converted into relative values $\delta(q_1)$ by calculation of an appropriate reference, i.e., the isolated NH_4^+ cation for ^{15}N and TMS for H. The values of $\delta(q_1)$ were calculated traditionally for the optimized minimum geometries as well as for the dynamically corrected structures.

Results

NMR Results. All parameters obtained by line shape analysis of the solid state ^{15}N NMR spectra of **2** and **3** are assembled in Table 1. Variable temperature experiments down to 120 K did not show any significant spectral changes although the sensitivity was improved. The experiments reported in this section were, therefore, arbitrarily carried out at 190 K as best compromise between sensitivity and ease of operation.

H/D-Isotope Effects on the Isotropic ^{15}N Chemical Shifts of 2 and 3. The ^{1}H decoupled ^{15}N CPMAS NMR spectra of **2-*h*** to **3-*d*** and those of the free acid **4** and the salt **5** are depicted in Figure 2. **4** contributes a signal at 145 ppm and **5** at 283 ppm with respect to external $^{15}NH_4Cl$.[22] In other words, the ^{15}N chemical shifts of this class of compounds are very sensitive to the N···H distance. We note that the ^{15}N chemical shift of a 0.4 M solution of KCN in water is 247 ppm.[23]

Table 1. Parameters of Chemical Shielding and Dipolar Coupling in **2-*h*** to **3-*d***[b]

		3-*h*: N1	**3-*h***: N2	**2-*h***
δ_{iso}(MAS)	[ppm]	189	219	205
δ_{11}	[ppm]	348 (2)	390 (2)	368 (2)
δ_{22}	[ppm]	341 (5)	387 (5)	361 (4)
δ_{33}	[ppm]	−117 (5)	−117 (5)	−104 (6)
α_{CSA}	[deg]			
β_{CSA}	[deg]			
r_c(NH)	[Å]	1.16	1.49	1.29
r(NH)	[Å]	1.18	1.50	1.31
$r_{N\cdots N}$(NMR)	[Å]	2.68		2.62
$r_{N\cdots N}$(XRD)[a]	[Å]			2.57
		3-*d*: N1	**3-*d***: N2	**2-*d***
δ_{iso}(MAS)	[ppm]	1.85	222	204
δ_{11}	[ppm]	341 (4)	395 (3)	366 (2)
δ_{22}	[ppm]	336 (5)	391 (5)	363 (2)
δ_{33}	[ppm]	−125 (6)	−125 (6)	−112 (6)
α_{CSA}	[deg]			
β_{CSA}	[deg]	7 (5)	4 (9)	8 (1)
r_c(ND)	[Å]	1.13 (1)	1.55 (5)	1.28 (1)
r(ND)	[Å]	1.15	1.56	1.30
$r_{N\cdots N}$(NMR)	[Å]	2.71		2.60

[a] Data from ref 15. [b] r_c(ND): cubic average distances N···D obtained by line shape analysis (see eq 8), r_c(NH): cubic average N···H distances extrapolated using eq 9; r(NH): mean distances calculated using eq 9. δ values are referenced to external solid $^{15}NH_4Cl$. δ_{iso}(MAS): isotropic ^{15}N chemical shifts obtained from the MAS spectra. α_{CSA}, β_{CSA}: Euler angles relating the CSA and dipolar ND coupling tensors.

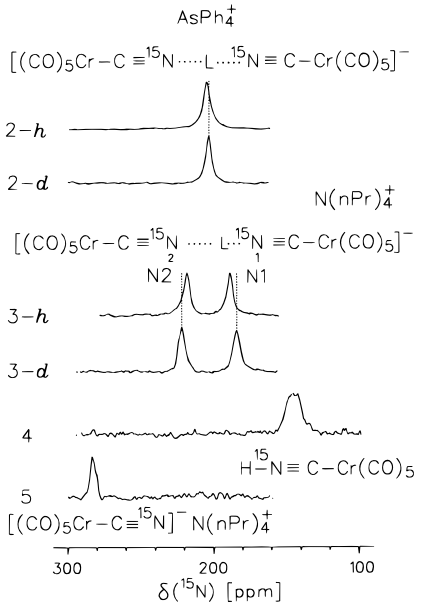

Figure 2. 9.12 MHz ^{15}N {^{1}H} CPMAS NMR spectra of compounds **2-*h*** to **3-*d***, **4**, **5** (Scheme 2) at room temperature, 2 kHz spinning speed, 9 μs 90° pulses. No dependence of temperature was observed. Adapted from ref 14.

By contrast, **2-*h*** gives rise to a single line at 205 ppm,[14,15] indicating that the two nitrogen atoms are equivalent. In other words, the two N···H distances are effectively equal within the NMR time scale. This finding is in agreement with the observation by X-ray crystallography of a C_2-symmetry of **2-*h***,[15] exhibiting a very short N···N distance of 2.569(7) Å. As depicted in Figure 2, deuteration of the symmetric bridge leads to a small high field shift of the ^{15}N signal to 204 ppm in the case of **2-*d***.

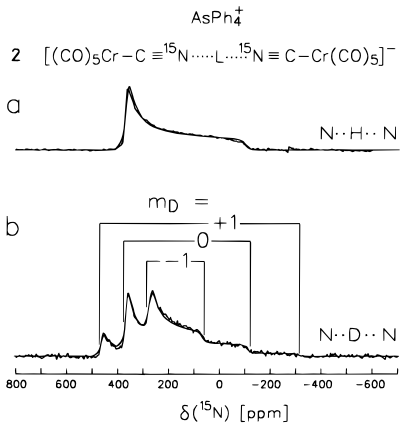

Figure 3. Superposed experimental and calculated 9.12 MHz ^{15}N-{^{1}H} CP NMR spectra of static solid powder samples of **2-*h*** (a) and **2-*d*** (b) at 190 K. For the simulation of spectrum (b) a H/D fraction of 35/65 had to be taken into account. The horizontal brackets indicate the width of the subspectra which belong to the spin quantum numbers for the attached deuterium atom, $m_D = +1$, 0, and −1, respectively.

On the other hand, **3-*h*** gives rise to two signals at 219 and 189 ppm,[14,15] indicating that the symmetry of the hydrogen bond is lifted when the countercation is changed. In other words, the proton density distribution function is no longer symmetric with respect to the hydrogen bond center. Now, deuteration of the asymmetric bridge has a large effect on the ^{15}N chemical shifts as shown in Figure 2:[14,15] the signal of the high-field nitrogen atom N1 shifts to higher and the signal of the low-field nitrogen atom N2 to lower field; i.e., we observe the isotope shifts of $^1\Delta^{15}$N1(D) = $\delta(^{15}$N1−H) − $\delta(^{15}$N1−D) = − 3 ppm and $^1\Delta^{15}$N2(D) = $\delta(^{15}$N2−H) − $\delta(^{15}$N2−D) = 4 ppm. The superscript 1 indicates that the ^{15}N atom experiencing the shift is one bond away from the deuteration site, according to the usual nomenclature.[11] These findings indicate that the shorter nitrogen−hydron distance is further decreased, and the larger distance increased upon deuteration. We note that in our previous studies of N−H···N hydrogen bonded solids slow to ultrafast proton-transfer processes were observed involving kinetic hydrogen/deuterium isotope effects,[2] but one-bond H/D isotope effects on ^{15}N chemical shifts could never be detected. Therefore, kinetic H/D isotope effects are typical for high and moderate barriers and H/D isotope effects typical for low-barrier hydrogen bonds, as found recently for asymmetric N···H···O hydrogen bonds in the liquid state.[13b]

Static ^{15}N NMR Spectra of 2 and 3 and Determination of N···D Distances in 2-*d* and 3-*d*. The ^{1}H decoupled static ^{15}N CP NMR spectrum of polycrystalline **2-*h*** (Figure 3a) shows the typical pattern for a nucleus with a quasi-axially symmetric tensor for the chemical shielding anisotropy (CSA). This corresponds to the local $C_{\infty v}$ symmetry of the cyano ligand where the high field component σ_{33} is oriented parallel to the C−N axis, while the two other components σ_{11} and σ_{22} are almost equivalent and orientated perpendicular to this axis.

The signal of **2-*d*** is additionally split into three subpatterns because of the dipolar ^{15}N−D interaction, corresponding to the three possible magnetic quantum numbers, $m_D = +1$, 0, and −1, for the attached deuterium atom (Figure 3b). By line shape simulation of the spectrum, one obtains the cubic average N···D distances r_c(ND) as well as the Euler angles α_{CSA} and β_{CSA} that orientate the N−D vector in the principal axis system of the

(22) The ^{15}N chemcal shift of a 5.6 M solution of $^{15}NH_4Cl$ in water is −353 ppm with respect to liquid nitromethane, see: (a) Witanowski, M.; Stefaniak, L.; Webb, G. A. *Annual Reports on NMR Spectroscopy, 11B*; Academic Press: New York, 1981. (b) Martin, G.; Martin, M. L.; Gouesnard, J. P. *NMR Basic Principles and Progress*; Springer: Heidelberg, Germany, 1989; Vol. 18 *^{15}N NMR Spectroscopy*.

(23) Wasylishen, R. E. *Can. J. Chem.* **1982**, *60*, 2194.

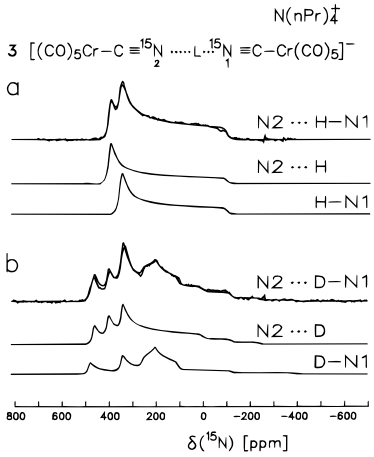

Figure 4. Superposed experimental and calculated 9.12 MHz ^{15}N-{^{1}H} CP NMR spectra of static solid powder samples of **3-*h*** (a) and **3-*d*** (b) at 190 K. The calculated spectra are the sum of the subspectra shown below the corresponding spectrum. These subspectra arise from the two nonequivalent ^{15}N atoms of **3-*h*** and **3-*d***, respectively.

CSA tensor. Because of the axial symmetry, σ_{33} is located parallel to the C−N axis; β_{CSA} then corresponds to the C−N−H bond angle, while α_{CSA} cannot be determined because of the similarity of σ_{11} and σ_{22}. β_{CSA} is found to be 8(1)°, and the two equivalent cubic average N···D distances r_c(N1···D) = r_c(N2···D) = 1.28(1) Å. We note that within the margin of error residual **2-*h*** could not be detected.

In the case of **3-*h*** the ^{1}H decoupled static ^{15}N NMR spectrum (Figure 4a) consists of two subspectra, each of which is similar to the spectrum of the symmetric compound **2-*h***. By line shape analysis the chemical shielding tensor components of N1 and N2 are obtained. As indicated in Table 1, σ_{33} does not differ significantly in **2-*h*** and **3-*h***, in contrast to $\sigma_{11} \approx \sigma_{22}$ which depend in a sensitive way on the symmetry of the bridge. These components are responsible for the increase of the isotropic chemical shift values when the ^{15}N···H distance is increased.

Again, **3-*d*** exhibits additional signal features arising now from a different dipolar interaction of the two ^{15}N atoms with the attached deuteron (Figure 4b). As the dipolar coupling constant is $\sim r^{-3}$, the splitting is larger for N1 than for N2. The line shape simulation of the spectrum leads to two sets of distances and Euler angles, β_{CSA} = 7(5)°, r_c(N1···D) = 1.13(1) Å and β_{CSA} = 4(9)°, r_c(N2···D) = 1.55(5) Å for N1 and N2, respectively. We note already here that the corresponding distances r_c(N1···H) and r_c(N2···H) included in Table 1 were obtained by chemical shift extrapolation as described below.

Results of Quantum Mechanical Calculations. Geometries and energies from ab initio MP2/6-31+G(d,p) calculations performed on **1-*h*** and **1-*d*** for selected fixed distances C2···Li, and the results of the subsequent IGLO calculations of NMR chemical shifts are presented in Tables 2 and 3, respectively. Part of this work was published in a preliminary paper.[14] All results refer to the optimized geometries of the [C≡N···H···N≡C]$^-$ subunit in the inhomogeneous electric field of Li$^+$. A global energy minimum was obtained at a distance C2···Li of 1.9637 Å, corresponding to the species C≡N−H···N≡C−Li exhibiting a polar covalent C−Li bond. Vibrational averaging of properties is restricted to the vibrational ground state. Higher vibrational levels were not taken into account as temperature effects on the experimental NMR parameters of **2** and **3** outside the margin of error could not be detected.

The influence of the C2···Li distance on the potential curves $V(q_1)$ of the collinear anharmonic hydron motion is depicted in Figure 5. The hydron positions q_1 are referred to the center of the hydrogen bond, but as the heavy atom positions are known from the calculations, the mean average and cubic average distances r_c(N···L) can easily be calculated, and the results which are different for L = H and D are included in Table 2. Different potentials are obtained for L = H, D due to the adiabatic approximation as is described in the theoretical section. This does not mean that the Born−Oppenheimer approximation is violated but that in a multidimensional dynamical treatment a different one-dimensional projection results for L = H and D.

When the C2···Li distance is short, an asymmetric N−H···N hydrogen bond is obtained, characterized by a single relatively

Table 2. Geometries and Energies from ab Initio MP2/6-31+G(d,p) Calculations of **1-*h*** and **1-*d*** [h]

C2···Li	**1.9637**	**3**	**5**	**7**	**9**	**11**	∞
N1···L [a]	1.0295	1.0404	1.0672	1.0860	1.0977	1.1068	1.1411
N1···N2 [a]	2.8312	2.7743	2.6851	2.6455	2.6257	2.6142	2.5790
N1···H [b]	1.0509	1.0668	1.1229	1.1814	1.2133	1.2298	1.2675
N2···H [b]	1.7630	1.6827	1.5171	1.3978	1.3436	1.3192	1.2675
N1···N2(H) [b]	2.8139	2.7495	2.6400	2.5792	2.5569	2.5490	2.5350
N1···H [c]	1.0398	1.0547	1.1065	1.1598	1.1902	1.2064	1.2491
N2···H [c]	1.7562	1.6747	1.5037	1.3772	1.3210	1.2961	1.2491
N1···N2(H) [c]	2.7960	2.7294	2.6102	2.5370	2.5112	2.5025	2.4982
E_0(H) [d]	−193.237307	−193.188084	−193.121570	−193.095977	−193.082309	−193.073653	−193.036587
ZPE(H) [e]	1498	1376	1088	825	680	606	444
N1···D [b]	1.0440	1.0581	1.1005	1.1438	1.1845	1.2111	1.2675
N2···D [b]	1.7757	1.6999	1.5560	1.4581	1.3887	1.3437	1.2675
N1···N2(D) [b]	2.8197	2.7580	2.6565	2.6019	2.5732	2.5548	2.5350
N1···D [c]	1.0365	1.0498	1.0903	1.1312	1.1700	1.1953	1.2491
N2···D [c]	1.7711	1.6946	1.5482	1.4458	1.3713	1.3247	1.2491
N1···N2(D) [c]	2.8076	2.7444	2.6385	2.5770	2.5413	2.5200	2.4982
E_0(D) [d]	−193.237314	−193.188099	−193.121645	−193.096174	−193.082481	−193.073721	−193.036587
ZPE(D) [e]	1090	990	810	655	524	442	274
ΔE_0 [f]	1.5	3.3	16.5	43.2	37.8	14.9	0
$\Delta(E_0 + \text{ZPE})$ [g]	410	389	295	213	194	179	170

[a] The distances refer to the optimized geometries for fixed C2···Li distances [Å]. [b] Dynamically corrected mean interatomic distances [Å]. [c] Dynamically corrected mean cubic interatomic distances [Å]. [d] E_0(L) total energy of the dynamically corrected structure [1 au = 219 474.63 cm^{-1} = 2625.500 kJ mol^{-1}]. [e] ZPE(L) zero-point energy [cm^{-1}] of the hydron L calculated for the collinear mode using an infinite mass for the heavy atoms [f] $\Delta E_0 = E_0$(H) − E_0(D) in cm^{-1}. [g] $\Delta(E_0 + \text{ZPE}) = E_0$(H) − E_0(D) + ZPE(H) − ZPE(D). [h] Additional geometry data for free CN−L are N1−L = 1.0003 Å ref *a*, N1−H = 1.0014 Å ref *b*, and N1−D = 1.0032 Å ref *b*. Some of the above results were reported in ref 14.

Table 3. IGLO Calculated ^{15}N, H, and D Chemical Shifts δ [ppm] of **1-*h***, **1-*d***, for Fixed C2−Li Distances [Å][a]

	C2−Li	**1.9637**	**3**	**5**	**7**	**9**	**11**	∞
(a)	δN1(H)$_{\parallel}$	−121.5	−121.8	−122.1	−122.2	−122.3	−122.3	−122.3
	δN1(H)$_{\perp}$	333.8	347.8	380.9	408.8	422.6	430.5	447.4
	δN1(H)	182.0	191.3	213.2	231.8	241.0	246.2	257.5
	δN2(H)$_{\parallel}$	−113.5	−117.0	−120.5	−121.6	−121.9	−122.0	−122.3
	δN2(H)$_{\perp}$	549.7	525.6	505.7	483.0	470.3	463.1	447.4
	δN2(H)	328.7	311.4	297.0	281.5	272.9	268.1	257.5
	δH$_{\parallel}$	−21.4	−21.5	−21.2	−20.9	−21.1	−21.1	−21.5
	δH$_{\perp}$	16.5	18.8	23.6	27.0	28.0	28.4	28.8
	δH	3.9	5.4	8.7	11.0	11.6	11.9	12.0
(b)	δN1(D)$_{\parallel}$	−121.5	−121.8	−122.0	−122.2	−122.3	−122.3	−122.3
	δN1(D)$_{\perp}$	332.5	345.65	373.7	395.8	412.8	425.1	447.4
	δN1(D)	181.1	189.8	208.5	223.1	234.4	242.6	257.5
	δN2(D)$_{\parallel}$	−113.4	−117.0	−120.4	−121.3	−121.8	−122.0	−122.3
	δN2(D)$_{\perp}$	551.1	527.6	511.4	490.3	479.1	467.8	447.4
	δN2(D)	329.6	312.8	300.5	289.0	278.5	271.1	257.3
	δD$_{\parallel}$	−15.6	−21.7	−21.6	−21.2	−21.2	−21.1	−21.5
	δD$_{\perp}$	16.1	18.2	22.5	25.5	27.2	28.1	28.8
	δD	3.5	4.9	7.8	9.9	11.1	11.7	12.0

[a] The δ values were calculated from the absolute chemical shieldings σ by $\delta = \sigma_{ref} - \sigma$, where $\sigma_{ref}(^{15}N) = 244.43$ was calculated for isolated NH_4+ and $\sigma_{ref}(^1H) = \sigma_{ref}(^2H)$ was calculated for isolated tetramethylsilane. The subscripts $\parallel$ and $\perp$ denote the components of the chemical shielding tensor orientated parallel and perpendicular to the molecular axis, respectively (cf. Figure 1). Additional ^{15}N chemical shift values are 369.8 ppm for Li−C≡N, 333.5 ppm for C≡N$^-$, 150.9 ppm for H−N≡C, and an ^{1}H chemical shift of 0.04 ppm for H−N≡C. Part of the above results were published in ref 14.

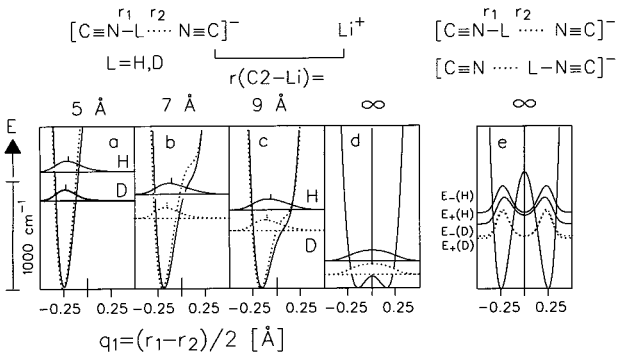

Figure 5. (a) to (d) calculated potential curves, vibrational ground-state energies, and squares of wave functions for the proton (full lines) and deuteron (dotted lines) motion in **1-*h*** and **1-*d***, respectively. The abscissa q_1 [Å] represents the distance between the hydron and the H-bond center which is the origin. The mean hydron positions $\langle q_1(L)\rangle$ are indicated by vertical lines, adapted from ref 14. (e) Sketch for the unrealistic case of coherent hydron tunneling in a double-well potential.

harmonic potential curve. The potential well is located close to the nitrogen atom N1 opposite to Li^+, thus minimizing the Coulomb energy between Li^+ and N≡C$^-$ (Figure 5a). As C2··· Li is increased, the hydron potential well shifts in the direction of the hydrogen bond center and the anharmonicity of the potential becomes maximal (Figure 5 (parts b and c)). Further increase of the C2−Li distance leads to a symmetric H-bond with a low barrier double well potential (Figure 5d).

The question for the effect of proton tunneling in the H-bond of **1** can be answered as follows. The barrier for the hydron motion in [C≡N···H···N≡C]$^-$ is lower than the vibrational ground state (Figure 5d). To achieve an increased barrier for the hydron motion (Figure 5e) it is necessary to increase artificially the N···N distance to a nonstationary region. In this case the lowest vibrational levels would occur in pairs exhibiting an energy splitting $E_-(L)$-$E_+(L)$ corresponding to a tunnel splitting. Moreover, the tunnel effect requires a symmetric double well potential which is an idealized case where perturbing fields of the surrounding ions are artificially switched off. Thus, proton tunneling in **1** is unrealistic and was, therefore, not considered further.

The asymmetry of the potential for intermediate C2···Li distances (Figure 5 (parts b and c)) leads to strong H/D isotope effects on the mean hydron positions $\langle q_1(L)\rangle$ and generally on the geometry of the H-bond but also the increase of the barrier (Figure 5 (parts d and e)).

As can be inferred from Table 2, the mean cubic N···H distances are slightly smaller than the mean linear distances r. In good approximation both quantities are related by the linear equation

$$r_c(N\cdots L) = 0.9877 r(N\cdots L) \qquad (9)$$

which was used to correct the experimental data, included in Table 1. Note that neither contributions of the bending zero-point vibration nor deviations of the hydrogen bond angle from 180° were taken into account.

Distance-Chemical Shift Correlation. In this section we are interested in a relation between the ^{15}N chemical shifts of **1** to **3** and the mean cubic nitrogen−hydron distances r_c. In the lower curve of Figure 6a we have plotted the isotropic ^{15}N NMR chemical shifts of **2-*d*** and **3-*d*** as a function of the experimental cubic average N···D distances r_c(ND); the upper curve contains the calculated values for **1-*h*** and **1-*d***. It was found that the data could well be described by the empirical function

$$\delta(^{15}N) = a - c\exp(-dr_c) \qquad (10)$$

with the fit parameters $a_{cal} = 327.88$ ppm, $c_{cal} = 4488$ ppm, $d_{cal} = 3.3174$ Å^{-1} leading to the upper solid line in Figure 6a. a_{cal} is close to the calculated value of 333.5 ppm for CN$^-$, whereas the calculated value for LiCN is shifted to lower field, i.e., 369.8 ppm where the Li···C bond is polar but covalent. Subsequently, the experimental data were also fitted to eq 10 leading to the lower solid line in Figure 6, with $a_{exp} = 235.4$ ppm, $c_{exp} = 1779.5$ ppm, and $d_{exp} = 3.1547$ Å^{-1}. a_{exp} is close to the value of the cyanide ion in water; by contrast, the covalent bond Cr···C bond in **5** induces a shift to lower field as in the case of LiCN. Using the assumption that the data for the protonated compounds **2-*h*** and **3-*h*** obey the same correlation, we extrapolated from ^{15}N chemical shifts the values r_c(NH) =1.29 Å for **2-*h*** and 1.16 and 1.49 Å for **3-*h*** (see Table 1).

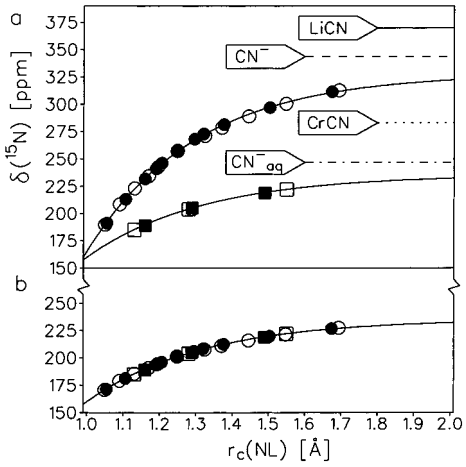

Figure 6. Correlation of the isotropic ^{15}N chemical shifts δ with the cubic average distances r_c(NL) (L = H, D) in **1**, **2**, and **3**. □: experimental values for **2**-***d***, **3**-***d***; ■: extrapolated values for **2**-***h*** and **3**-***h***. ●: calculated values for **1**-***h***. ○: calculated values for **1**-***d***. (a) unscaled and (b) scaled calculated values and experimental values. The solid lines were calculated as described in the text. The unscaled calculated values of LiCN and CN^- are depicted in (a) as well as the experimental value of CN^- in water according to ref 23 and the value of **5** according to Figure 2, abbreviated as CrCN.

The absolute difference between the calculated values obtained for **1** and the experimental values for **2** and **3** is not surprising in view of the different systems. Moreover, the calculations do not consider any intermolecular or crystal interactions. Nevertheless, using the fit parameters of Figure 6a one can scale the calculated values using the equation

$$\delta_{\mathrm{cal}}^{\mathrm{scaled}} = a_{\mathrm{exp}} - c_{\mathrm{exp}}\left(\frac{a_{\mathrm{cal}} - \delta_{\mathrm{cal}}}{c_{\mathrm{cal}}}\right)^{\frac{d_{\mathrm{exp}}}{d_{\mathrm{cal}}}} \qquad (11)$$

in such a way that they coincide within the margin of errors with the experimental values. The result is shown in Figure 6b. We note that the scaling factors obtained also scale the calculated value of the cyanide anion to the experimental value. In the following, only the ^{15}N chemical shifts, scaled in this way, are further discussed which is especially important when comparing H/D isotope effects on the ^{15}N chemical shifts.

We did not succeed in this study to measure experimentally ^{1}H and ^{2}H NMR chemical shifts of polycrystalline **2** and **3**. Therefore, the calculated values which are included in Table 3 were not corrected in a way similar to the ^{15}N data.

Discussion

Using high resolution and dipolar ^{15}N solid-state NMR, we have evaluated the H/D isotope effects on the geometry of the strong N···H···N − hydrogen bonded units in the anions of **2** and **3** (Scheme 2) as a function of the countercation. As the units are at least 6.8 Å away from each other[15] they can be treated in good approximation as uncoupled. Therefore, we modeled the effects observed by ab initio calculations of the geometries and of the ^{15}N chemical shielding tensors of isolated $[C{\equiv}N{\cdots}H{\cdots}N{\equiv}C]^-{\cdots}Li^+$ (**1-*h*)** and its deuterated analogue **1-*d***. Using an iterative procedure the optimized geometries for the anions for fixed distances to the Li^+ countercation were calculated, by accounting for the different dynamics of the proton and the deuteron. In the absence of an electric field created by the Li^+-countercation the hydron motion takes place in a symmetric double-well potential (Figure 5d); however, the barrier is lower than the zero-point energies (ZPE) of the proton and of the deuteron. The situation depicted in Figure 5e where the barrier is larger than the ZPE does not correspond to an optimized geometry for the anion but to a situation where the N···N distance is artificially increased. In the presence of the electric field—created by reducing the distance to Li^+—the hydrons move in asymmetric single well potentials (Figure 5a–c). Therefore, the hydrogen bond geometries were well defined in all cases and not complicated by a fast proton-transfer equilibrium which should have led to temperature-dependent effects. A global energy minimum for **1** is obtained at a C···Li distance of 1.9637 Å, where the C−Li bond corresponds to a polar covalent bond. Using this model, the effects of the countercation on the hydrogen bonds of the compounds **2** and **3** (Scheme 2) could be modeled, which induce a symmetric hydrogen bond in **2** but an asymmetric bond in **3**.

In this section we discuss the information arising from those results which provide snapshots of proton transfer in low-barrier hydrogen bonds. In the first part we consider the isotope effects on the hydrogen bond geometries and the zero-point energies and in the second part how these effects are related to the NMR chemical shifts. These relations are important as in usual liquid state NMR experiments distance information cannot directly be obtained, in contrast to H/D isotope effects on chemical shifts.[13b]

Hydrogen Bond Geometries. Distance Correlation for N···H···N Hydrogen Bonds. A hydrogen bond geometry correlation can be obtained from the concept of bond valence–bond length well established in chemistry.[8,25] This concept predicts that the two hydrogen bond distances r_1 and r_2 in Scheme 1 cannot be varied independently, i.e., that they are correlated. This means that q_1 should also be correlated with q_2. In the following, some mathematical equations are derived in order to show that other hydrogen bond properties can be correlated with q_1 and q_2 as well.

The bond order or valence p of a diatomic molecule AH is defined according to Pauling[25a] by

$$p = \exp\{-(r-r_0)/b\} \qquad (12)$$

where r_o indicates the equilibrium A···H distance. p is unity at $r = r_o$ and zero at infinite distance; b indicates the increase in the distance where p has decreased to $1/e$. A hydrogen bonded system A−H···B is characterized by two bond valences p_1 and p_2 and two distances r_1 and r_2. The bond valence concept then assumes that the total bond order of hydrogen is unity

$$p_1 + p_2 = \exp\{-(r_1-r_0)/b\} + \exp\{-(r_2-r_0)/b\} = 1 \qquad (13)$$

It follows that

$$r_2 = r_0 - b\ln[1 - \exp\{-(r_1-r_0)/b\}] \qquad (14)$$

The parameter b can be expressed as

$$b = [(r_1+r_2)_{\mathrm{min}} - 2r_0]/2\ln 2 \qquad (15)$$

Here, $(r_1+r_2)_{\mathrm{min}}$ represents a minimum value which is equal to the minimum distance A···B in the case of a linear hydrogen bond. At this point the valence of each bond is $^1/_2$.

The validity of eq 14 was demonstrated by Steiner et al. for N···H···N[8b] and O···H···O[8a] hydrogen bond units in crystals

(24) Allen, F. H.; Davies, J. E.; Galloy, J. J.; Johnson, O.; Kennard, O.; Macrae, C. F.; Mitchell, E. M.; Mitchell, G. F.; Smith, J. M. Watson, D. G. *J. Chem. Inf. Comput. Sci.* **1991**, *31*, 187.

(25) (a) Pauling, L. *J. Am. Chem. Soc.* **1947**, *69*, 542. (b) Brown, I. D. *Acta Crystallogr*. **1992**, *B48*, 553.

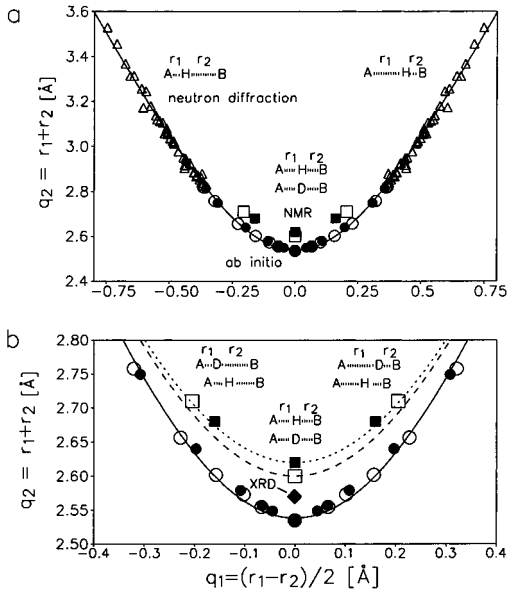

Figure 7. (a) Correlation of the hydrogen bond length $q_2 = r_1 + r_2$ with the proton-transfer coordinate $q_1 = {}^1/_2(r_1 - r_2)$. Δ: neutron diffraction data;[8b,26] □: experimental values for **2-*d***, **3-*d***; ■: extrapolated values for **2-*h*** and **3-*h***. ●: calculated values for **1-*h***. ○: calculated values for **1-*d***. (b) Expansion of (a), ◆: abscissa value from NMR and ordinate value from X-ray diffraction according to ref 15. The dotted and dashed lines were fitted to the experimental values for the protonated and deuterated compounds of **2** and **3**, respectively. For further explanation see text.

on the basis of a number of neutron diffraction structures contained in the Cambridge Structural Data Base.[24,26] Similar correlations were discussed by Gilli et al.[8c] For our purposes we rewrite eq 14 as follows

$$q_2 = r_1 + r_2 = 2r_0 + 2q_1 + 2b \ln[1 + \exp\{-2q_1/b\}] \quad \text{with} \quad q_1 = {}^1/_2(r_1 - r_2) \tag{16}$$

where q_1 represents the deviation of the hydron from the hydrogen bond center and q_2 the heavy atom distance in the case of a linear hydrogen bond (see Scheme 1).

In the remainder of this discussion we will show that additional hydrogen bond properties can be described in terms of this simple model, i.e., in terms of the first, second, and third derivatives

$$\frac{dq_2}{dq_1} = 2\frac{1 - \exp\{-2q_1/b\}}{1 + \exp\{-2q_1/b\}}$$

$$\frac{d^2q_2}{dq_1^2} = \frac{8}{b}\frac{\exp\{-2q_1/b\}}{(1 + \exp\{-2q_1/b\})^2}$$

$$\frac{d^3q_2}{dq_1^3} = -\frac{16}{b^2}\frac{\exp\{-2q_1/b\}(1 - \exp\{-2q_1/b\})}{(1 + \exp\{-2q_1/b\})^3}$$

Correlation between q_1 and q_2. Figure 7 shows a plot of q_1 vs q_2 for the neutron diffraction data of various linear and nonlinear NHN-hydrogen bonds reported by Steiner,[8b] some additional neutron data,[26] the dynamically corrected *ab initio* values for the model compounds **1-*h*** and **1-*d***, and the experimental data for **2-*h***, **2-*d*** and **3-*h***, **3-*d***. The correlation indicates that a hydrogen bond compression occurs simultaneously as the proton is transferred from one heavy atom to the other. The solid line was calculated by fitting the data to eq 16, resulting in the parameters $r_0 = 0.990$ Å and $b = 0.404$ Å, i.e., $q_{2\min} = 2.54$ Å. These values are close to those of Steiner[8b] who, based on weakly hydrogen bonded NHN systems, found $r_0 = 0.996$ Å and $b = 0.381$ Å, i.e., $q_{2\min} = 2.52$ Å. We note that the neutron crystallographic data and the theoretical data for **1** all refer to a situation of an effective single well potential for the hydron motion, which renders the surprisingly good correlation understandable.

The N···N distance of **2-*h*** is 2.57 Å (see Table 1 and ref 15, route in Figure 7b) and, therefore, close to the minimum value 2.54 Å. The small difference may either indicate that the proton-transfer barrier in **2** is slightly larger than proposed in Figure 5d for **1**, i.e., a situation similar to Figure 5e, or that the hydrogen bond is not completely linear. The larger NMR values $r_1 + r_2$ of 2.62 and 2.60 Å in **2-*h*** and **2-*d*** (Table 1) point into the same direction. In addition, also the data of the asymmetric hydrogen bond of **3-*h*** and **3-*d*** are located slightly above the correlation curve as depicted in Figure 7b.

Finally, we note that a larger barrier for the hydron motion than indicated in Figure 5d can only explain the slightly larger N···N distance observed by X-ray diffraction for **2-*h*** but not the larger distances observed by NMR. In this symmetric case the hydron density function has two equal maxima with a small density at the hydrogen bond center. The average cubic N···H or N···D distance obtained by dipolar NMR is given in a point approximation by the sum of two terms

$$1/r_c^3 = 0.5/r_1^3 + 0.5/r_2^3 \tag{18}$$

As r_2 can be calculated using eq 14 as a function of r_1, one can calculate using eq 18 the values $q_2 = 2r_c$ determined by NMR as a function of the sum $r_1 + r_2$. E.g., for $r_1 = 1.02$ Å, i.e., $r_2 = 2.06$ Å or $r_1 + r_2 = 3.08$ Å we obtain a much smaller value of $2r_c = 2.47$ Å. When $r_1 + r_2$ is decreased, $2r_c$ increases monotonically until both values become equal when $r_1 + r_2$ reaches the minimum. Thus, the observation by dipolar NMR of a much smaller distance $r_1 + r_2$ as compared to the crystallographic N···N distance can be used as a criterion for a fast proton transfer through a barrier. Note, however, that there are also other solid-state NMR methods for detecting ultrafast proton transfers between nitrogen atoms, i.e., proton-transfer modulated longitudinal ^{15}N relaxation and chemical shift analysis.[14] E.g., in the case of a fast proton-transfer equilibrium the splitting of the two ^{15}N lines of Figure 2 should have been dependent on temperature, in contrast to the experimental finding.

Primary and Secondary Geometric Hydrogen Bond Isotope Effects. We now come to a discussion of the H/D isotope effects on the NHN−hydrogen bond geometry. It is clear that replacement of H by D can lead to a change of q_1 and of q_2 i.e.

$$\Delta q_1 = q_1(\mathrm{H}) - q_1(\mathrm{D}) = {}^1/_2[r_{1(\mathrm{H})} - r_{2(\mathrm{H})} - r_{1(\mathrm{D})} + r_{2(\mathrm{D})}] \tag{19}$$

(26) To obtain numerical data, the search of the Cambridge Structural Data Base[24] (CSD) performed by Steiner[8b] was repeated with version 5.1 and the same search criteria. Retrieved were 40 N−H···N bonds in 27 crystals, CSD reference codes: ADENOS01, AMBACO07, AMCLPY11, AMXBPM10, ANILPC, ARGIND11, CADKEX01, CBOATZ02, CYACHZ01, CYGUAN01, CYTOSH, DMSDIM01, FORAMO01, HARMID03, HDRZHO11, IMAZOL04, IMAZOL06, IMAZOL13, LHISTD13, MATCQI09, MEADEN02, MELAMI04, MTHMAD11, NTRGUA01, PYRZOL02, TCQETA02, TRAZOL03.

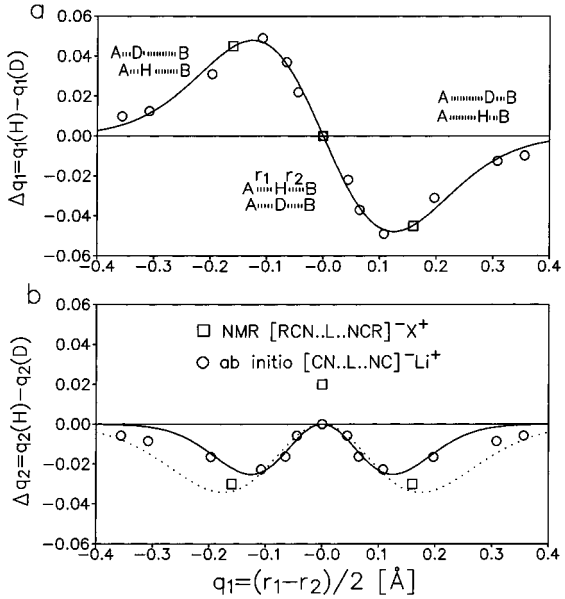

Figure 8. (a) Primary geometric isotope effect $\Delta q_1 = q_1(\mathrm{H}) - q_1(\mathrm{D})$ on the proton-transfer coordinate $q_1 = {}^1/_2(r_1 - r_2)$. o: dynamically corrected ab initio values for **1**; □: NMR data of **2** and **3**. (b) Secondary geometric isotope effect $\Delta q_2 = q_2(\mathrm{H}) - q_2(\mathrm{D})$ on the hydrogen bond length $q_2 = r_1 + r_2$. For the calculation of the solid and dotted lines see text.

and

$$\Delta q_2 = q_2(\mathrm{H}) - q_2(\mathrm{D}) = r_{1(\mathrm{H})} + r_{2(\mathrm{H})} - r_{1(\mathrm{D})} - r_{2(\mathrm{D})} \qquad (20)$$

We call Δq_1 the *primary* and Δq_2 the *secondary geometric hydrogen bond isotope effect*. In the case of a linear hydrogen bond Δq_2 corresponds to the change of the heavy atom distance upon deuteration, as discussed by Ubbelohde.[9] In this case Δq_2 can be determined using X-ray diffraction. The determination of the primary effect Δq_1 is much more difficult. In this study this quantity was determined by NMR and by ab initio calculations using a dynamic correction. For the subsequent discussion, both the calculated and experimental values of Δq_1 and Δq_2 are plotted in Figure 8a and 8b as a function of the proton-transfer coordinate $q_1 = {}^1/_2(r_1 - r_2)$. Δq_1 shows a dispersion-type behavior. It is positive when $q_1 < 0$ and negative for $q_1 > 0$, indicating that replacement of H by D leads always to a hydron shift away from the hydrogen bond center, i.e., shortens the covalent short N−L bond. At $q_1 = \pm\infty$ and $q_1 = 0$ there is no effect, i.e., $\Delta q_1 = 0$. The maximum and minimum values of Δq_1 are observed at $q_{1\mathrm{m}} = \pm\ 0.122$ Å in the anharmonic region corresponding to the potential curves for C2⋯Li = 5 and 7 Å (Figure 5).

The solid line in Figure 8a was calculated using the empirical equations

$$\Delta q_1 = 1.656 \times 10^{-5} \times \left(\frac{d^3 q_2}{dq_1^3}\right)\left(\frac{d^2 q_2}{dq_1^2}\right)^4 \text{Å} \qquad (21)$$

The agreement between the calculated and experimental data is excellent.

By contrast, the secondary isotope effect Δq_2 behaves in a different way. The calculated values are negative, i.e., deuteration increases always the heavy atom distance. Minima are observed in the same regions as found for Δq_1. The solid line in Figure 8b was calculated using the empirical relation

$$\Delta q_2 = -11.9\ \Delta q_1{}^2\ \text{Å} \qquad (22)$$

By contrast, the dotted line in Figure 8b was calculated by combination of eqs 16, 20, and 21, i.e., for the case where H/D substitution does not lead to a deviation from the correlation curve of Figure 7.

The calculated value of Δq_2 vanishes at $q_1 = 0$, whereas the experimental value found for **2** is even positive, as depicted in Figures 7b and 8b. This means that the N⋯N distance is shorter in **2-*d*** than in **2-*h*** whereas the calculated values for **1-*d*** and **1-*h*** are equal. Within the framework of this approximation no geometric H/D isotope effect can arise for a symmetric low-barrier hydrogen bond at $(r_1+r_2)_{\min}$ and $r_1 - r_2 = 0$, whereas a full theoretical two-dimensional treatment can lead to a small positive value of Δq_2 as has been shown by Almlöf[10d] for the isolated symmetric FHF^-/FDF^- anions. The slightly shorter distance F⋯F in FDF^- as compared to FHF^-, i.e., a *positive* geometric isotope effect can be explained with the smaller spatial width of the zero−point vibration of the former. Thus, the NHN^- hydrogen bond in **2** resembles the FHF^- case. In other words, a two-dimensional treatment of **1** could perhaps confirm this explanation. Nevertheless, bending modes and deviations from a hydrogen bond linearity could also play a role.

Isotopic Fractionation. In solution, often the only way to detect low-barrier hydrogen bonds is the measurement of H/D fractionation factors[5,7] which reflect zero-point vibrational energy changes between a standard state, generally water and the hydrogen bond site studied. Therefore, let us have a look at the calculated factors for **1** although they have not been measured for **2** and **3**. We note that as we have treated **1** as a linear system, bending vibrations are not included in the following discussion, nor entropy changes. The isotopic fractionation factors we are referring to are the equilibrium constants K of the H/D exchange reaction between the free and the hydrogen bonded molecules, i.e.

$$\mathrm{D{-}N{\equiv}C + Li{\cdots}C{\equiv}N{\cdots}H{-}N{\equiv}C}\ (\mathbf{1}\text{-}\boldsymbol{h}) \overset{K}{\rightleftharpoons} \mathrm{H{-}N{\equiv}C + Li{\cdots}C{\equiv}N{\cdots}D{-}N{\equiv}C}\ (\mathbf{1}\text{-}\boldsymbol{d}) \qquad (23)$$

Neglecting entropy changes and considering only the fundamental vibrational states, K is given in approximation by

$$K = \exp(-\Delta\mathrm{ZPE}/RT) \qquad (24)$$

where R is the gas constant, T is the temperature and, ΔZPE is the zero-point energy difference given by

$$\Delta\mathrm{ZPE} = \mathrm{ZPE(H{-}N{\equiv}C)} - \mathrm{ZPE(D{-}N{\equiv}C)} + E_0(\mathrm{D}) - E_0(\mathrm{H}) + \mathrm{ZPE(D)} - \mathrm{ZPE(H)} \qquad (25)$$

where E_0(L) is the energy of the equilibrium geometry of ***1*-L** and ZPE(L) the corresponding hydron zero-point energy, visualized partly in Figure 5 and included in Table 2. ZPE(H−N≡C) = 1819 cm^{-1} and ZPE(D−N≡C) = 1299 cm^{-1} are the hydron zero-point energies for the free acid L−N≡C, obtained from the ab initio calculations by using the harmonic approximation and an infinite mass for the N≡C group. ΔZPE can be fitted empirically to the equation

$$\Delta\mathrm{ZPE} = -0.172 \times \left(\frac{d^2 q_2}{dq_1^2}\right)^2\ \mathrm{kJ\ mol^{-1}} \qquad (26)$$

symbolized by the solid line in Figure 9a. At $q_1 = 0$ about 4 kJ mol^{-1} are lost as compared to the free acid. By combination

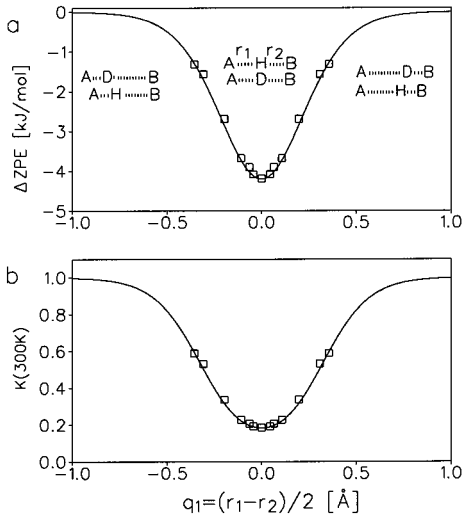

Figure 9. (a) Zero-point energy changes and (b) isotopic fractionation factors for the H/D exchange reaction eq 23 between the separated acid (CN−L) and the complex LiCN···L···NC **1** as a function of the proton-transfer coordinate $q_1 = {}^1/_2(r_1-r_2)$. For the calculation of the solid lines see text.

with eq 24 one can calculate the isotopic fractionation factor K as a function of q_1, depicted in Figure 9b where we choose a temperature of 300 K. When $q_1 \ll 0$, i.e., the hydrogen bond is very asymmetric, and the hydron potential is harmonic, $K = 1$, i.e., no isotopic fractionation occurs. However, at $q_1 = 0$, in the region of the symmetric low-barrier hydrogen bond, the fractionation factor decreases to about 0.19. This is because of the well-known fact that H is enriched in the environment with the smaller zero-point energy.[7] The graph of Figure 9b resembles the graph calculated by Huskey[7d] for the isotopic fractionation of the $CH_3OHOCH_3^-$ anion, who found a minimum value of K of about 0.27. The two results are, however, not directly comparable as Huskey included all vibrations but was interested in the case of a fixed distance O···O, i.e., a fixed value of q_2. Allowing a variation of the latter would then probably also lower the minimum value of K.

Hydrogen Bond Properties and NMR Chemical Shifts. The last problem addressed in this paper is how the findings of Figures 7−9 can be translated into NMR chemical shielding information available by liquid state NMR, where dipolar interactions or molecular structures cannot be easily obtained.

Chemical Shift-Distance Correlations. In Figure 6 we had already established an experimental and theoretical correlation between the ^{15}N NMR chemical shifts $\delta(^{15}\text{N})$ and the mean cubic nitrogen−hydron distance r_c. Here we plot in Figure 10 (parts a and b) the mean ^{15}N chemical shift

$$\bar{\delta} = [\delta(^{15}\text{N1}) + \delta(^{15}\text{N2})]/2 = 194.6 + 1.425\frac{d^2q_2}{dq_1^2} \quad (27)$$

and the half difference

$$\Delta\delta = [\delta(^{15}\text{N1}) - \delta(^{15}\text{N2})]/2 = 19.5\frac{dq_2}{dq_1} \quad (28)$$

of the two nitrogen atoms of **1**−**3** as a function of q_1. $\bar{\delta}$ is a linear function of the second derivative exhibiting a small low field shift in the case of the symmetric hydrogen bond. By contrast, $\Delta\delta$ is a linear function of the first derivative. The values for $q_1 \rightarrow \pm\infty$, $\bar{\delta} = 194.6$ and $\Delta\delta = \pm 40.7$, correspond to the values that can be obtained with eq 10 (experimental

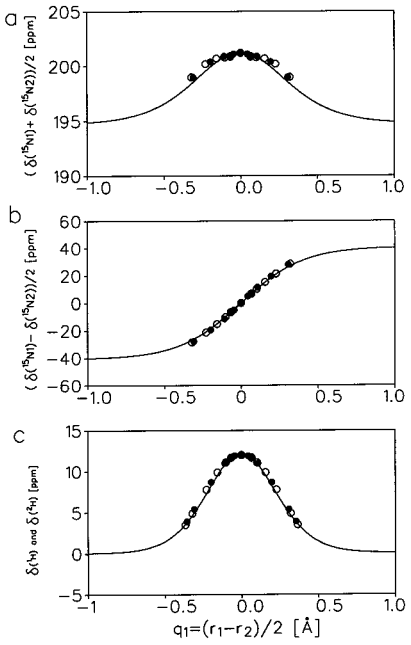

Figure 10. Correlation of the mean ^{15}N chemical shifts $\bar{\delta} = [\delta(^{15}\text{N1}) + \delta(^{15}\text{N2})]/2$ (a), the half difference $\Delta\delta = [\delta(^{15}\text{N1}) - \delta(^{15}\text{N2})]/2$ (b) and the ^{1}H and ^{2}H NMR chemical shifts (c) as a function of the proton-transfer coordinate $q_1 = {}^1/_2(r_1-r_2)$ for the results of ab initio calculations for **1-*h*** (●), **1-*d*** (○). For the calculation of the solid lines see text.

curve in Figure 6) for $r_c = 0.977$ and $r_c \rightarrow \infty$, respectively. In Figure 10c we have plotted the unscaled calculated ^{1}H chemical shifts as a function of q_1 and can fit the data to

$$\delta(^1\text{H}) = 0.04 + 0.0769q_2^2\left(\frac{d^2q_2}{dq_1^2}\right)^2 \text{ kJ mol}^{-1} \quad (29)$$

leading to the solid line in Figure 10c. Experimentally, one may not have the distances but only the ^{1}H and ^{15}N chemical shifts.[13b] A plot of both values leads to the correlation curve $\delta(^1\text{H}) = f(\delta(^{15}\text{N}))$ depicted in Figure 11a, where the solid line was generated by combining eqs 27−29. A similar curve was obtained previously in the case of a low-temperature NMR study of hydrogen bonded complexes between carboxylic acids and pyridine dissolved in a deuterated Freon.[13b]

Isotope Effects on Chemical Shifts. As $\delta(^{15}\text{N})$ is a measure of q_1 it is not surprising that isotope effects on the ^{15}N chemical shift $^1\Delta^{15}\text{N(D)} = \delta(^{15}\text{N}\cdots\text{D}) - \delta(^{15}\text{N}\cdots\text{H})$ plotted in Figure 11b as a function of $\delta(^{15}\text{N})$ behave qualitatively in a similar way as the *primary geometric isotope effects* Δq_1 of Figure 8a. Moreover, the unscaled primary H/D isotope effects on the hydron chemical shifts, i.e., $\delta(^1\text{H}) - \delta(^2\text{H})$ plotted in Figure 11c behave as the *secondary geometric isotope effects* Δq_2 of Figure 8b. The solid lines in Figure 11 (parts b and c) were calculated from combination of eqs 16, 22, 23, and 27−30. The agreement with the calculated data is satisfactory.

Fractionation Factors as a Function of ^{15}N Chemical Shifts. Finally, by combination of eqs 16, 17, 27−30 we obtain a correlation between ΔZPE or the fractionation factors and the nitrogen chemical shifts as indicated by the solid lines in Figure 12 (parts a and b) which resemble the plots of Figure 9. Thus, after proper reparametrization the above equations may be useful for liquid−state NMR studies. We note, however, that the assumption of a similar environment for all molecules is not fulfilled in the liquid state. This is because the electric field

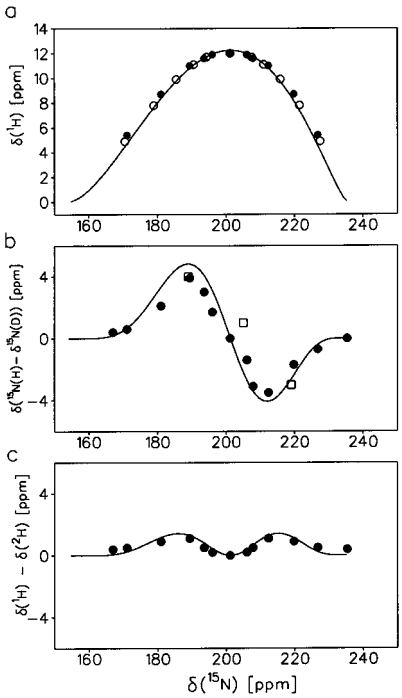

Figure 11. (a) ^{1}H (●) and ^{2}H NMR (○) chemical shifts, (b) primary H/D isotope effects on the ^{15}N chemical shifts, and (c) secondary one bond H/D isotope effects on the ^{2}H chemical shifts as a function of the ^{15}N chemical shifts. Results of ab initio calculations for **1**-***h***, **1**-***d*** are indicated by circles, the experimental values for **2**-***h***, **3**-***h*** and **2**-***d***, **3**-***d*** by squares, respectively. For the calculation of the solid lines see text.

produced by the solvent molecules at the hydrogen bond depends on the environment and on temperature[13d] which complicates the analysis of the temperature dependence of fractionation factors.

Conclusions

We have shown that high resolution and dipolar ^{15}N solid-state NMR is capable of determining H/D isotope effects on the hydron (L = H, D) and heavy atom locations in strong NLN−hydrogen bonds. At the same time, ab initio calculations and subsequent solution of the Schrödinger equation of the nuclear motion in related model complexes followed by quantum-mechanical chemical shift calculations are an essential tool in order to interpret the experimental results. Thus, the combination of NMR spectroscopy and theoretical methods can

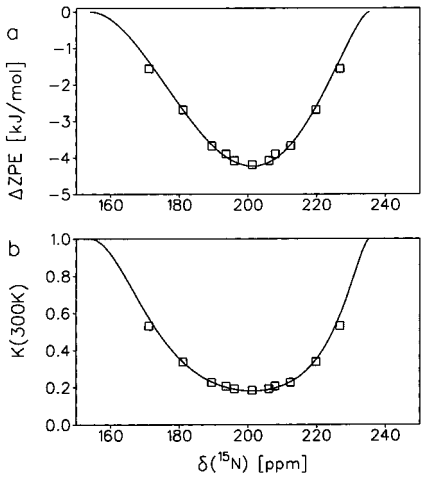

Figure 12. (a) Energies and (b) equilibrium constants *K* for the H/D exchange reaction eq 23 between the separated acid (CN−L) and base (LiCN) and one of the LiCN···L···NC complexes **1** as a function of the ^{15}N chemical shifts. For the calculation of the solid lines see text.

shed new light on the geometry of strong low-barrier hydrogen bonds which cannot easily be studied using diffraction methods. Two kinds of geometric isotope effects have been determined experimentally and theoretically, the *primary* one referring to the hydron position in the bridge and the *secondary* one to the position of the heavy atoms of the bridge. The data are interpreted starting from a correlation between the two heavy atom-hydron distances of NHN-hydrogen bonded systems observed by Steiner et al.,[8b] established by neutron crystal structure. This correlation is corroborated here for the so far missing case of the strongest hydrogen bonds and is reproduced by the theoretical calculations. The following hydrogen bond properties, i.e., the *primary* and *secondary* geometric hydrogen bond isotope effects, fractionation factors, ^{1}H and ^{15}N chemical shifts, and H/D isotope effects on the chemical shifts, can be expanded empirically as a function of various differentials of the above hydrogen bond correlation.

Acknowledgment. In Berlin, this work was supported by the Kommission für Forschung und Wissenschaftlichen Nachwuchs der Freien Universität Berlin and the Fonds der Chemischen Industrie, Frankfurt. Some of us thank Prof. R. L. Schowen, Lawrence, Kansas, and Prof. G. S. Denisov, St. Petersburg, Russia for helpful discussions.

JA9719790